

SUPPLEMENTARY INFORMATION

Supplementary Methods

Chemicals and materials. Oleic acid (Sigma-Aldrich) and 10%BSA (essentially fatty acid free, Sigma-Aldrich) were used to make a 7.5 mM stock solution (5:1 oleic acid:BSA molar ratio)³¹. BODIPY493/503 was from Invitrogen.

Cell culture. *Drosophila* S2 cells were cultured in Schneider's *Drosophila* medium (Invitrogen) supplemented with 10% fetal bovine serum and antibiotics (100 unit/ml penicillin and 100 µg/ml streptomycin) at 25°C as described³². RNAi treatment of S2 cells were performed as previously described¹⁰. A segment of pBluescript backbone was used as the template for control RNAi (referred as control RNAi thereafter). Transfection of S2 cells was performed using Cellfectin reagent (Invitrogen). Images of live cells were taken using LSM 510 confocal microscope (Carl Zeiss MicroImaging) with a 63× oil immersion lens.

For Arf/COP1 specificity experiments (Figure 4), controls included knockdowns of COPII (*sar1*, *sec12*, *sec24* and *sec13*), clathrin (*Chc* and *Clc*), other ARFs (ARF4: *Arf102F*, ARF6: *Arf51F*, ARL1: *Arf72A*, ARL2: *Arf84F* and ARL3: *CG6560*), GEFs (*sec71* and *CG31158*), and GAPs (*ArfGAP1* and *Gap69C*).

Electron microscopy. RNAi treated cells were cultured with 1 mM oleate incubation for 24 hours, fixed in 1.5% glutaraldehyde, 4% polyvinylpyrrolidone, 0.05% calcium chloride, 0.1M sodium cacodylate, pH 7.4, on ice, and then pelleted. The samples were stained for lipid using an imidazole-buffered osmium tetroxide method³³, then block-stained in 2% uranyl acetate overnight at 4°C, dehydrated, infiltrated and embedded in LX-112 resin (Ladd Research Industries). Samples were sectioned ultrathin (65 nm) on a Reichert Ultracut S ultramicrotome and stained with 0.8% lead citrate. Grids were examined on a JEOL JEM-1230 electron microscope (JEOL, USA Inc.) and photographed using the Gatan Ultrascan 1000 digital camera (Gatan, Inc.).

Visual image analyses of the RNAi screen. Both the first (15,683 genes; whole genome) and second (847 repeated genes) data sets were scored visually by the same two independent observers who were blinded to gene identities. In total, nearly 95,000 images (15,643 genes, with 6 images per gene), each with several hundred cells, were examined visually. For visual scoring, a MATLAB script was utilized that allowed lipid droplets in each image (six per gene) to be scored for three criteria: number (more, normal, fewer), size (smaller, normal, larger), and dispersion (more, normal, less). These scores were imported to a spreadsheet to compile a hit list. In the first round of visual scoring, hits were defined as those genes identified as abnormal by both observers. The same observers and procedures were used in the visual screen of the repeat data set.

Automated image analyses. Both the initial and repeat data sets were analyzed by automated image analysis. DAPI and BODIPY images from the initial screen were analyzed by using a series of MATLAB scripts (for a detailed description see http://mpibcms.biochem.mpg.de/en/rg/lipidrophe/absatz_01.html). In short, DAPI images were used to segment the images into individual cells by using Otsu's thresholding³⁴ and watershed segmentation from the image processing toolbox. Similarly, the BODIPY signal outline was determined by thresholding. The cell shapes were overlaid on the BODIPY image and several parameters of the BODIPY signal (*e.g.*, size, intensity, and numbers of clusters) were measured and averaged per cell, excluding cells at the boundary of the image and cell clumps. Images with few cells were flagged, as were images with abnormal DAPI signals. Among the parameters, the total signal per image, and the number of clusters and the mean signal per cell proved most useful and were further used for statistical analysis. In particular, for descriptive statistics, the interquartile range (IQR) was determined for the values of each parameter and conditions that resulted in a signal more than 1.5 deviant from the lower (0.25) or higher (0.75) percentile were considered hits for this category. Lists of hits for each category were compiled in a spreadsheet and compared with the results from visual screening.

Quantitative PCR. dsRNAs (16 µg) were added to individual wells of 6-well plates. After 4 days, cells were harvested and lysed in RNA-Stat-60 (Tel-test). Total RNA (1.5µg) was used to synthesize first-strand cDNAs by using SuperscriptIII reverse transcriptase and random hexamer primers (Invitrogen).

Real-time quantitative PCR was performed with the ABI Perkin Elmer Prism 7700 (Applied Biosystems) and SYBR green detection of amplified products. Each 25 μ l PCR reaction mix contained 2 μ l cDNA, 12.5 μ l 2x SYBR Green master mixture (Qiagen) and 600 nM of primers (*midway* forward: 5'-CCAAGCTGGTGCAATATCCT-3', *midway* reverse: 5'-CACCAACCTCCAATAAACGCT-3', *Arf79F* forward: 5'-GTCGCCTGGATGTACCAGTT-3', *Arf79F* reverse: 5'-GTATCGGTGAGGCGAGAGAG-3', *Aldh* forward: 5'-GAGGGCCTACCCGGCTACT-3', and *Aldh* reverse: 5'-CTCCCTTGCAATGGTCATATCA-3'). *Aldh* (Aldehyde dehydrogenase)³⁵ was used as an internal reference gene.

***Saccharomyces cerevisiae* studies.** Strains examined were wild-type (Cry1, W303), a control strain (Δ 4) lacking neutral lipid synthesis enzymes (*Dga1*, *Lro1*, *Are1*, *Are2*) and lipid droplets (a gift from Sten Stymne), and Δ *arf1* (W303). Yeast strains were cultured in YPD media. At O.D.600 = 0.8, aliquots were taken from culture and BODIPY (1 μ g/ml) dye was added. Images were obtained with a LSM 510 confocal microscope (Carl Zeiss MicroImaging).

Endoribonuclease-prepared short-interfering RNA (esiRNA) treatment of hepatoma cells and HeLa cells. esiRNAs targeting ARF1 (mammalian homolog of *Arf79F*), GBF1 (mammalian homolog of *garz*), ARCN1 (mammalian homolog of δ *Cop*), FASN (mammalian homolog of FAS), SREBF1 (mammalian homolog of SREBP) and SCAP were generated with published methods^{36,37}. The endonuclease RNaseIII was a gift from Barbara Panning. Purified esiRNAs (20ng) were transfected with Lipofectamine (Invitrogen) into Huh7 human hepatoma cell line (provided by Melanie Ott) in 24-well plates. After culture for 40 h in DMEM medium, 1 mM oleate was added to the medium and cells were incubated for another 24 h. Cells were then stained with BODIPY and imaged with LSM 510 confocal microscope (Carl Zeiss MicroImaging). Similar approach was performed for HeLa cell RNAi treatment with the exception of transfection with DharmFECT (Dharmacon) for 30 h before loading with 1 mM Oleate.

References for Methods

31. Stone, S. J. et al. Lipopenia and skin barrier abnormalities in DGAT2-deficient mice. *J Biol Chem* **279**, 11767-76 (2004).
32. Clemens, J. C. et al. Use of double-stranded RNA interference in Drosophila cell lines to dissect signal transduction pathway. *Proc Natl Acad Sci U S A* **97**, 6499-503 (2000).
33. Angermüller, S. & Fahimi, H. D. Imidazole-buffered osmium tetroxide: An excellent stain for visualization of lipids in transmission electron microscopy. *Histochem. J.* **14**, 823–835 (1982).
34. Otsu, N. A threshold selection method from gray-level histograms. *IEEE Trans Syst Man Cybern* **9**, 62-66 (1979).
35. Seegmiller, A. C. et al. The SREBP pathway in Drosophila: regulation by palmitate, not sterols. *Dev Cell* **2**, 229-38 (2002).
36. Yang, D. et al. Short RNA duplexes produced by hydrolysis with Escherichia coli RNase III mediate effective RNA interference in mammalian cells. *Proc Natl Acad Sci U S A* **99**, 9942-7 (2002).
37. Kittler, R., Heninger, A. K., Franke, K., Habermann, B. & Buchholz, F. Production of endoribonuclease-prepared short interfering RNAs for gene silencing in mammalian cells. *Nat Methods* **2**, 779-84 (2005).
38. Cermelli, S., Guo, Y., Gross, S. P., Welte, M.A. The lipid-droplet proteome reveals that droplets are a protein-storage depot. *Curr Biol.* **16**, 1783-95 (2006).

Supplementary Materials

Table S1. Genes with dramatically altered lipid droplet morphology identified in screen.

Table S2. Genes with moderately altered lipid droplet morphology identified in screen.

Table S3. Genes identified in screen by automated analysis

Movies

Movie S1 Projection movie of S2 cells loaded with oleate.

Movie S2 Projection movie of *Cct1* knockdown cells loaded with oleate.

Figures

Fig. S1. Knock down of selected genes by RNAi treatment. (a) *Drosophila* S2 cells were treated with 500-bp dsRNA for 3 days to knockdown with control RNAi (middle column) or *midway* (right column). RNA was extracted and the mRNA levels for *midway* were measured by real time-PCR and compared with those from control cells (middle column). (b) The mRNA expression level for knockdown of *Arf79F* was analyzed analogously to (a). (** P < 0.00001 vs control)

Fig. S2. Lipid droplets fuse in cells with knockdown of *Cct1*. S2 cells were treated with RNAi as described for the screen, incubated with 1mM oleate-containing medium, and imaged by confocal time-lapse microscopy. Images shown span 30 min and show three-dimensional projections of a lipid droplet before (left), during (middle), and after fusion (right).

Fig. S3. Ultrastructure of control and *mdy*, *Arf79F* and *Cct1* knockdown cells after oleate loading.

Cells were treated with RNAi for 3 days, then incubated with medium containing 1mM oleate for 24 h, and prepared for electron microscopy as described in Methods. Representative images are shown.

Fig. S4. Phenotypes of ARF1 deletion in yeast and ARF1 knockdown in human hepatoma (HuH7) cells and HeLa cells. (a) HuH7 cells were treated with esiRNA against ARF1 (mammalian homolog of *Arf79F*), GBF1 (mammalian homolog of *garz*), ARCN1 (mammalian homolog of *δCop*), FASN (mammalian homolog of FAS), SREBF1 (mammalian homolog of SREBP), SCAP or a control esiRNA for 40 h and then incubated with 1 mM Oleate for 24 h, fixed and stained for lipid droplets with BODIPY.

Representative confocal sections are shown. (b) HeLa cells were treated with esiRNA against control, ARF1 or GBF1 for 30 h and loaded with 1mM Oleate for 24 h, stained for droplets with BODIPY and imaged on confocal microscope. The overall transfection efficiency for esiRNA was low (~10% for HuH7 cells and 50% for HeLa cells). Shown in (a) and (b) are representative images that were selected on the basis of droplet phenotypes that were similar to those observed in *Drosophila* cells and not in control knockdown cells. (c) Live yeast cells with *ARF1* deletion were stained with BODIPY and imaged by confocal microscopy. Controls were wild-type yeast (left) and Δ4 (middle), a strain with deletions of four enzymes of neutral lipid synthesis (*Dgal*, *Lro1*, *Are1*, and *Are2*) that was kindly provided by Dr. S. Stymne

(Uppsala, Sweden). Droplets were more numerous in *ARF1* deletion mutants. Scale bar = 10 μm in (a), 5 μm in (b) and 3 μm in (c).

Fig. S5. Effect of BFA on droplet formation in *Drosophila* S2 cells. Two representative cells are shown for each condition. Lipid droplets were stained by BODIPY and Golgi stacks were stained with anti-*Drosophila* Golgi antibody (CalBiochem). Pre-treatment of 10 $\mu\text{g}/\text{ml}$ BFA for 30 minutes before oleate loading leads to collapse of Golgi stacks and droplet phenotype similar to ARF1/COPI knockdowns.

Table S1. Genes with dramatically altered lipid droplet morphology identified in screen

Class I Fewer lipid droplets		
CG#	Symbol	Function
CG10370	Tbp-1	endopeptidase activity
CG31991	mdy	diacylglycerol O-acyltransferase activity
CG1395	stg	protein tyrosine/serine/threonine phosphatase activity
CG5363	cdc2	cyclin-dependent protein kinase activity
CG5940	CycA	cyclin-dependent protein kinase regulator activity
CG8975	RnrS	ribonucleoside-diphosphate reductase activity
CG10484	Dox-A2	endopeptidase activity
CG4904	Pros35	endopeptidase activity
CG3329	Prosbeta2	endopeptidase activity; threonine endopeptidase activity
CG10938	ProsMA5	endopeptidase activity
CG7762	Rpn1	endopeptidase activity
CG1341	Rpt1	endopeptidase activity; ATPase activity
CG16916	Rpt3	endopeptidase activity
CG3455	Rpt4	endopeptidase activity
CG3328		caspase activity
CG7425	eff	ubiquitin-protein ligase activity
CG32744	Ubi-p5E	protein binding
CG7292	Rrp6	3'-5' exonuclease activity
CG32782	tlk	protein serine/threonine kinase activity
CG8877	prp8	RNA splicing factor activity
CG5352	SmB	RNA splicing factor activity
CG10753	snRNP69D	RNA splicing factor activity
CG1249		RNA splicing factor activity
CG4849	eEF2	translation elongation factor activity
CG14641		mRNA binding; nucleic acid binding
CG3578	bi	RNA polymerase II transcription factor activity
CG7951	sima	RNA polymerase II transcription factor activity
CG7552	CG33967	unknown

Class II Smaller size lipid droplets, more dispersed		
CG#	Symbol	Function
CG10859		motor activity; dynein complex
CG10822		ATPase activity, coupled; dynein complex
CG8732	* l(2)44DEa	long-chain-fatty-acid-CoA ligase activity
CG8055	shrb	carrier activity
CG4916	me31B	ATP-dependent RNA helicase activity
CG6718		calcium-independent phospholipase A2 activity
CG1318	Hexo1	beta-N-acetylhexosaminidase activity; hydrolase activity
CG1100	Rpn5	endopeptidase activity
CG9454		serine-type endopeptidase inhibitor activity
CG5119	* pAbp	poly(A) binding
CG11276	* RpS4	structural constituent of ribosome; nucleic acid binding
CG6501	Ngp	GTP binding; receptor binding
CG31196	14-3-3epsilon	DAG-activated phospholipid-dep. protein kinase C inhibitor
CG3889	CSN1b	small GTPase regulator activity; signalosome

CG18332	CSN3	unknown; signalosome
CG2038	CSN7	unknown; signalosome
CG5179	Cdk9	cyclin-dependent protein kinase activity
CG7035	Cbp80	RNA cap binding
CG3180	RpII140	DNA-directed RNA polymerase activity
CG7885	RpII33	DNA-directed RNA polymerase activity
CG6711	Taf2	RNA polymerase II transcription factor activity
CG7957	MED17	RNA polymerase II transcription mediator activity
CG13867	MED8	RNA polymerase II transcription mediator activity
CG18009	Trf2	RNA polymerase II transcription factor activity
CG1343	Sp1	RNA polymerase II transcription factor activity
CG7664	crp	RNA polymerase II transcription factor activity
CG31666		transcription factor activity
CG2252	fs(1)h	DNA binding; protein kinase activity
CG4817	Ssrp	single-stranded DNA binding; single-stranded RNA binding
CG9007		protein binding; zinc ion binding
CG4429	Rbp2	translation initiation factor activity; mRNA binding
CG9075	eIF-4a	translation initiation factor activity
CG9677	Int6	translation initiation factor activity
CG9769	eIF3-S5	translation initiation factor activity
CG32104		ATP binding; ATPase activity; calcium ion binding
CG1715	I(3)03670	unknown
CG6729		unknown
CG9170		unknown
CG9578		unknown
CG10933		unknown
CG14220		unknown
CG15009	ImpL2	unknown

Class III Normal/larger size lipid droplets, more dispersed

CG#	Symbol	Function
CG8385	Arf79F	GTP binding; GTPase activity
CG8487	garz	ARF guanyl-nucleotide exchange factor activity
CG7961	alphaCop	binding; protein transporter activity; COPI complex
CG6223	betaCop	binding; COPI complex
CG6699	beta'Cop	protein transporter activity; COPI complex
CG14813	deltaCOP	COPI complex
CG1528	gammaCop	binding; COPI complex
CG3948	zetaCOP	COPI complex

Class IV Normal/larger size lipid droplets, highly condensed

CG#	Symbol	Function
CG8053	eIF-1A	translation initiation factor activity
CG4153	eIF-2beta	translation initiation factor activity
CG8636	eIF3-S4	translation initiation factor activity
CG4954	eIF3-S8	translation initiation factor activity
CG4878	eIF3-S9	translation initiation factor activity
CG7490	RpLPO	DNA-(apurinic or apyrimidinic site) lyase activity; ribosome hydro-lyase activity; oxidoreductase activity
CG5844		

Class V Fewer lipid droplets, larger size

CG#	Symbol	Function
CG1049	Cct1	choline-phosphate cytidylyltransferase activity
CG18330	Cct2	choline-phosphate cytidylyltransferase activity
CG2201	CK	choline kinase activity; ethanolamine kinase activity
CG8522	HLH106	transcription factor activity; SREBP
CG33131	SCAP	sterol regulatory element binding-protein (SREBP) cleavage
CG3523	FAS	fatty-acid synthase activity

Ribosomal protein encoding genes [1]

CG#	Symbol	Function
CG12275	RpS10a	structural constituent of ribosome; nucleic acid binding
CG8332	* RpS15	structural constituent of ribosome; nucleic acid binding
CG8922	RpS15a	structural constituent of ribosome; nucleic acid binding
CG12324	* RpS15Ab	structural constituent of ribosome; nucleic acid binding
CG8900	* RpS18	structural constituent of ribosome; nucleic acid binding
CG15693	* RpS20	structural constituent of ribosome; nucleic acid binding
CG15697	RpS30	structural constituent of ribosome; nucleic acid binding
CG14792	sta	structural constituent of ribosome; nucleic acid binding
CG8857	RpS11	structural constituent of ribosome; nucleic acid binding
CG2033	* RpS15Aa	structural constituent of ribosome; nucleic acid binding
CG4046	* RpS16	structural constituent of ribosome; nucleic acid binding
CG3922	* RpS17	structural constituent of ribosome; nucleic acid binding
CG4464	* RpS19a	structural constituent of ribosome; nucleic acid binding
CG8415	RpS23	structural constituent of ribosome; nucleic acid binding
CG3751	RpS24	structural constituent of ribosome; nucleic acid binding
CG6779	* RpS3	DNA-(apurinic or apyrimidinic site) lyase activity; ribosome
CG2168	* RpS3A	structural constituent of ribosome; nucleic acid binding
CG10944	* RpS6	structural constituent of ribosome; nucleic acid binding
CG7808	* RpS8	structural constituent of ribosome; nucleic acid binding
CG5920	* sop	structural constituent of ribosome; nucleic acid binding
CG17521	RpL10	structural constituent of ribosome; nucleic acid binding
CG7283	RpL10Ab	structural constituent of ribosome; nucleic acid binding
CG4651	* RpL13	structural constituent of ribosome; nucleic acid binding
CG1475	RpL13A	structural constituent of ribosome; nucleic acid binding
CG3203	RpL17	structural constituent of ribosome; nucleic acid binding
CG8615	RpL18	structural constituent of ribosome; nucleic acid binding
CG6846	RpL26	structural constituent of ribosome; nucleic acid binding
CG4759	RpL27	structural constituent of ribosome; nucleic acid binding
CG15442	RpL27A	structural constituent of ribosome; nucleic acid binding
CG12740	RpL28	structural constituent of ribosome; nucleic acid binding
CG1821	RpL31	structural constituent of ribosome; nucleic acid binding
CG7939	RpL32	structural constituent of ribosome; nucleic acid binding
CG4111	* RpL35	structural constituent of ribosome; nucleic acid binding
CG7622	RpL36	structural constituent of ribosome; nucleic acid binding
CG5502	* RpL4	structural constituent of ribosome; nucleic acid binding
CG2960	RpL40	structural constituent of ribosome; nucleic acid binding
CG11522	RpL6	structural constituent of ribosome; nucleic acid binding

CG4897	RpL7	structural constituent of ribosome; nucleic acid binding
CG3314	RpL7A	structural constituent of ribosome; nucleic acid binding
CG1263	RpL8	structural constituent of ribosome; nucleic acid binding
CG6141	RpL9	structural constituent of ribosome; nucleic acid binding

Note: * previously identified from Drosophila embryonic lipid droplet proteome (ref. 37)

[1] A subset of the most striking genes (41 of the 132) encoded ribosome components and associated proteins. These genes showed a distinct phenotype with more dispersed droplets similar to Class III. However, phase contrast images of these knockdowns revealed decreased cell numbers and multiple large vacuolar structures throughout the cells, suggesting that the cells may not be healthy. It is presently not clear whether these genes involved in protein synthesis are directly involved in lipid droplet biology, or whether their knockdowns result in a non-specific effect on cell viability.

Table S2 Genes with moderately altered lipid droplet morphology identified in screen

Class I Fewer lipid droplets		
CG#	Symbol	Function
CG3938	CycE	cyclin-dependent protein kinase regulator activity
CG10800	Rca1	unknown
CG11888	Rpn2	endopeptidase activity
CG1404	* ran	GTPase activity; protein binding; GTP binding
CG16792	DebB	RNA splicing factor activity
CG2189	Dfd	RNA polymerase II transcription factor activity
CG8264	Bx42	unknown
CG12750	ncm	unknown

Class II More lipid droplets, smaller size and more dispersed		
CG#	Symbol	Function
CG3887		selenium binding
CG12235	Arp11	structural constituent of cytoskeleton; actin binding
CG9750	rept	DNA helicase activity
CG17821		acyltransferase activity
CG17654	Eno	phosphopyruvate hydratase activity
CG9595	osm-6	microtubule motor activity; kinesin complex
CG7033	*	ATPase activity, coupled; unfolded protein binding
CG3018	lwr	ubiquitin-protein ligase activity
CG4320	raptor	binding; protein modification
CG11622	Rlip	Ral GTPase activator activity
CG4012	gek	protein serine/threonine kinase activity; small GTPase regulator
CG4700	Sema-2a	receptor activity
CG8606	RhoGEF4	Rho guanyl-nucleotide exchange factor activity
CG11870		protein serine/threonine kinase activity
CG12344		GABA receptor activity
CG13995		G-protein coupled receptor activity
CG17060	Rab10	GTPase activity
CG9575	* Rab35	GTPase activity
CG6197		transcription regulator activity
CG11266		mRNA binding; nucleotide binding
CG12267		DNA-directed RNA polymerase activity
CG12254	MED25	RNA polymerase II transcription mediator activity
CG3886	Psc	transcription regulator activity
CG11799	Mnf	transcription factor activity
CG17328		transcription regulator activity
CG10986	g	binding; intracellular transport
CG7861		protein folding
CG9636		unknown
CG8087		unknown
CG9432	I(2)01289	protein disulfide isomerase activity
CG13605		protein binding; zinc ion binding
CG31386		unknown
CG1524	RpS14a	structural constituent of ribosome; nucleic acid binding
CG8495	RpS29	structural constituent of ribosome; nucleic acid binding

CG1258 [1]	pav	microtubule motor activity; kinesin complex
CG13345 [1]	tum	Rho GTPase activator activity

Class IV Normal/larger size lipid droplets, condensed

CG#	Symbol	Function
CG2260		unknown
CG3992	srp	RNA polymerase II transcription factor activity

Class V Fewer lipid droplets, larger size

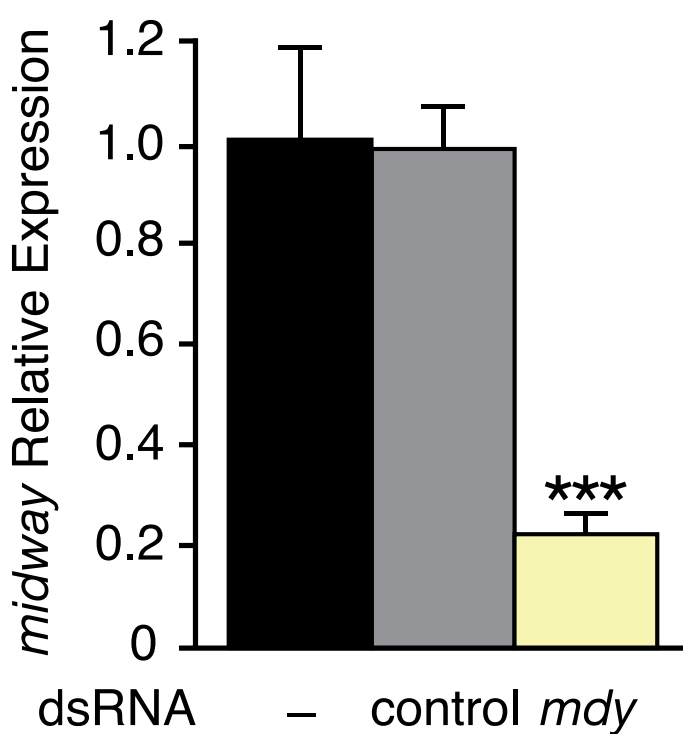
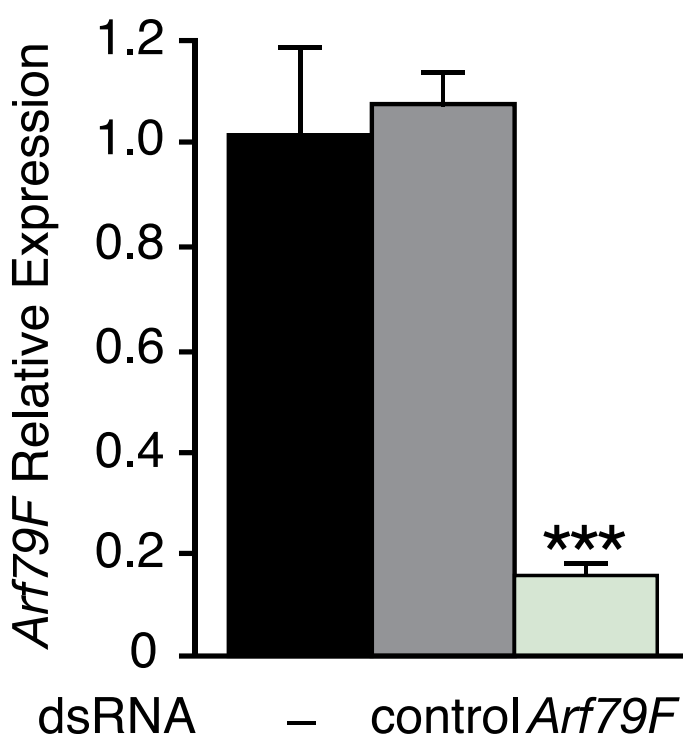
CG#	Symbol	Function
CG2503	atms	kinesin binding
CG11700	Ubiquitin	protein modification

Note: * previously identified from Drosophila embryonic lipid droplet proteome (ref. 37)
 [1] defect in cytokinesis, with large multinucleated cells

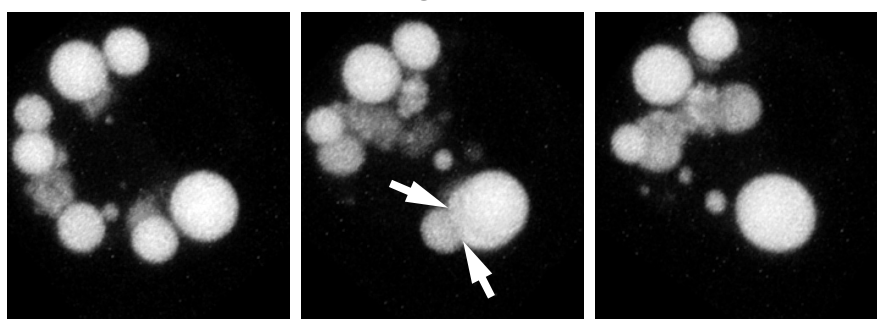
Table S3. Genes identified in screen by automated analysis

CG#	Note	Symbol	Function
CG17608	T	fu12	1-acylglycerol-3-phosphate O-acyltransferase activity
CG9390	T	AcCoAS	acetate-CoA ligase activity
CG7379	C		acetyltransferase activity; protein binding
CG10996	M		aldose 1-epimerase activity
CG9143	C		ATP-dependent RNA helicase activity
CG32465	T	CG34127	carboxylesterase activity
CG7094	T		casein kinase I activity
CG5452	M	dnk	deoxynucleoside kinase activity; ATP binding
CG16713	T		erine-type endopeptidase inhibitor activity
CG7440	T,M,C	tgy	galactosyltransferase activity
CG9042	T	Gpdh	glycerol-3-phosphate dehydrogenase (NAD+) activity
CG12530	T	Cdc42	GTPase activity
CG8287	M	Rab8	GTPase activity
CG3949	M	hoip	mRNA binding; structural constituent of ribosome
CG11027	T	Arf102F	NAD(P)+-protein-arginine ADP-ribosyltransferase activity
CG7368	T		nucleic acid binding; zinc ion binding
CG7054	T		phosphatidylethanolamine binding; kinase inhibitor activity
CG9060	T	Zpr1	protein binding; zinc ion binding
CG1210	M	Pk61C	protein serine/threonine kinase activity
CG9635	M	RhoGEF2	Rho guanyl-nucleotide exchange factor activity
CG7269	T	Hel25E	RNA helicase activity
CG7577	C	ppk20	serine-type peptidase activity
CG7352	T		structural constituent of cytoskeleton
CG7627	T,C		ATPase activity; transporter activity
CG15319	M	nej	transcription coactivator activity; acetyltransferase activity
CG6964	M	Gug	transcription corepressor activity
CG17888	T	Pdp1	transcription factor activity
CG7734	C	shn	transcription factor activity
CG9954	C	maf-S	transcription factor activity
CG10543	T		transcription regulator activity
CG7036	C	rno	transcription regulator activity
CG7372	C		transcription regulator activity
CG8950	T		transcription regulator activity
CG2238	M	Ef2b	translation elongation factor activity
CG9596	T		translation initiation factor activity
CG7375	T,C		ubiquitin-protein ligase activity
CG11132	M	DMAP1	unknown
CG16783	T	fzr2	unknown
CG30118	C		unknown
CG3885	M	sec3	unknown
CG5114	M		unknown
CG5308	C	dpr5	unknown
CG7085	T	I(2)s5379	unknown
CG7946	T		unknown
CG8309	T	Tango7	unknown
CG9047	T		unknown
CG9422	T		unknown

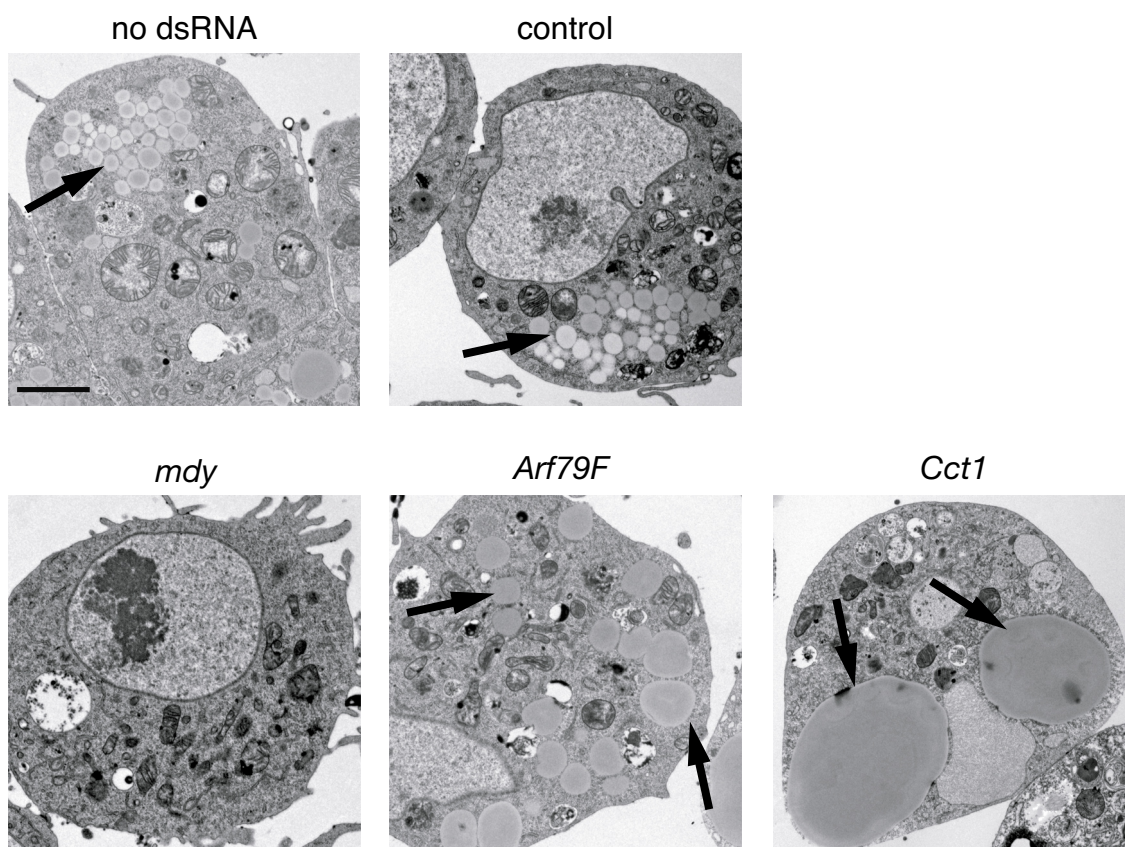
Note: T: altered total signal
 M: altered mean signal
 C: altered cluster number

a**b**Farese *et al*, Figure S1

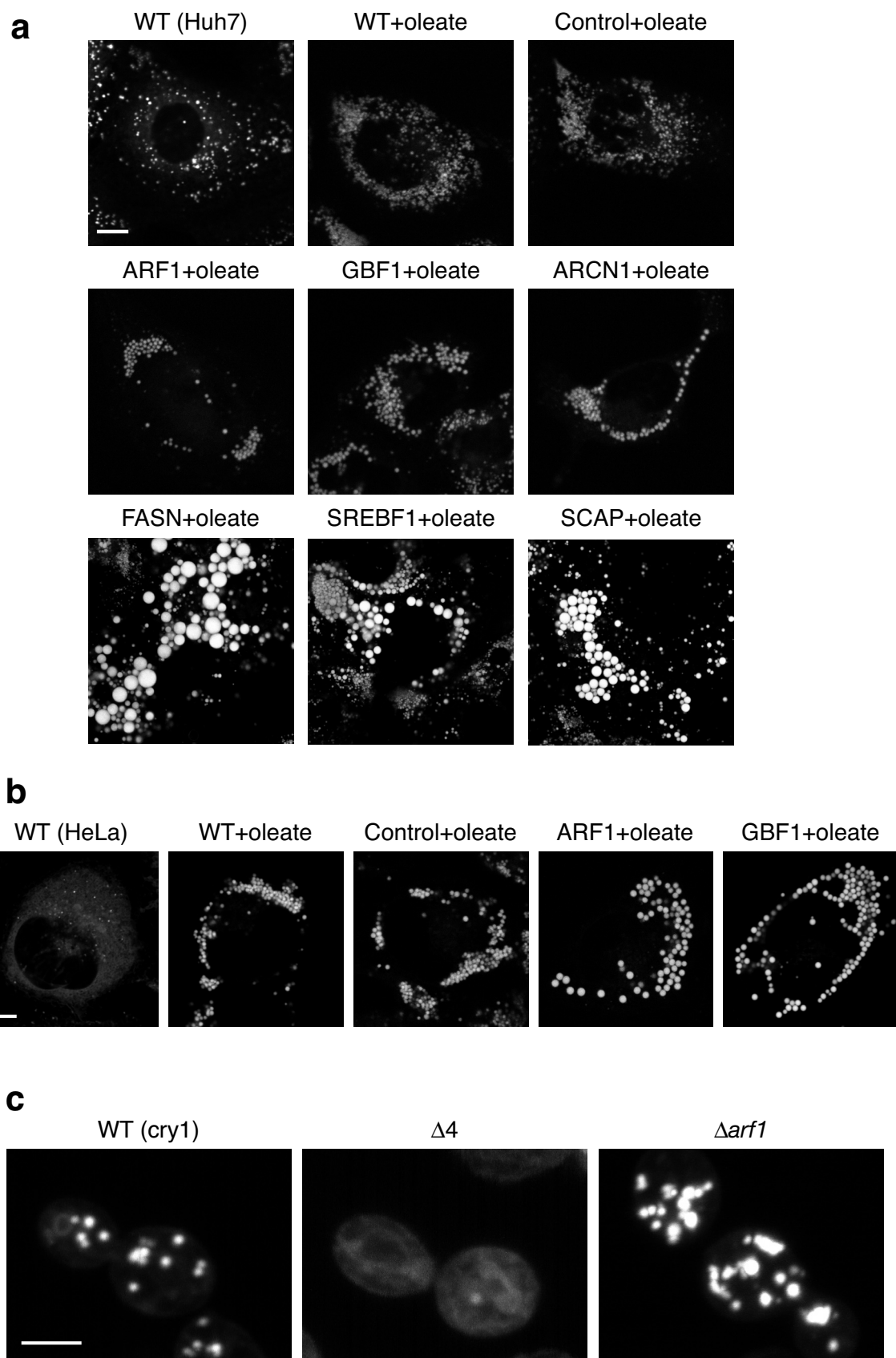
before fusion during fusion after fusion

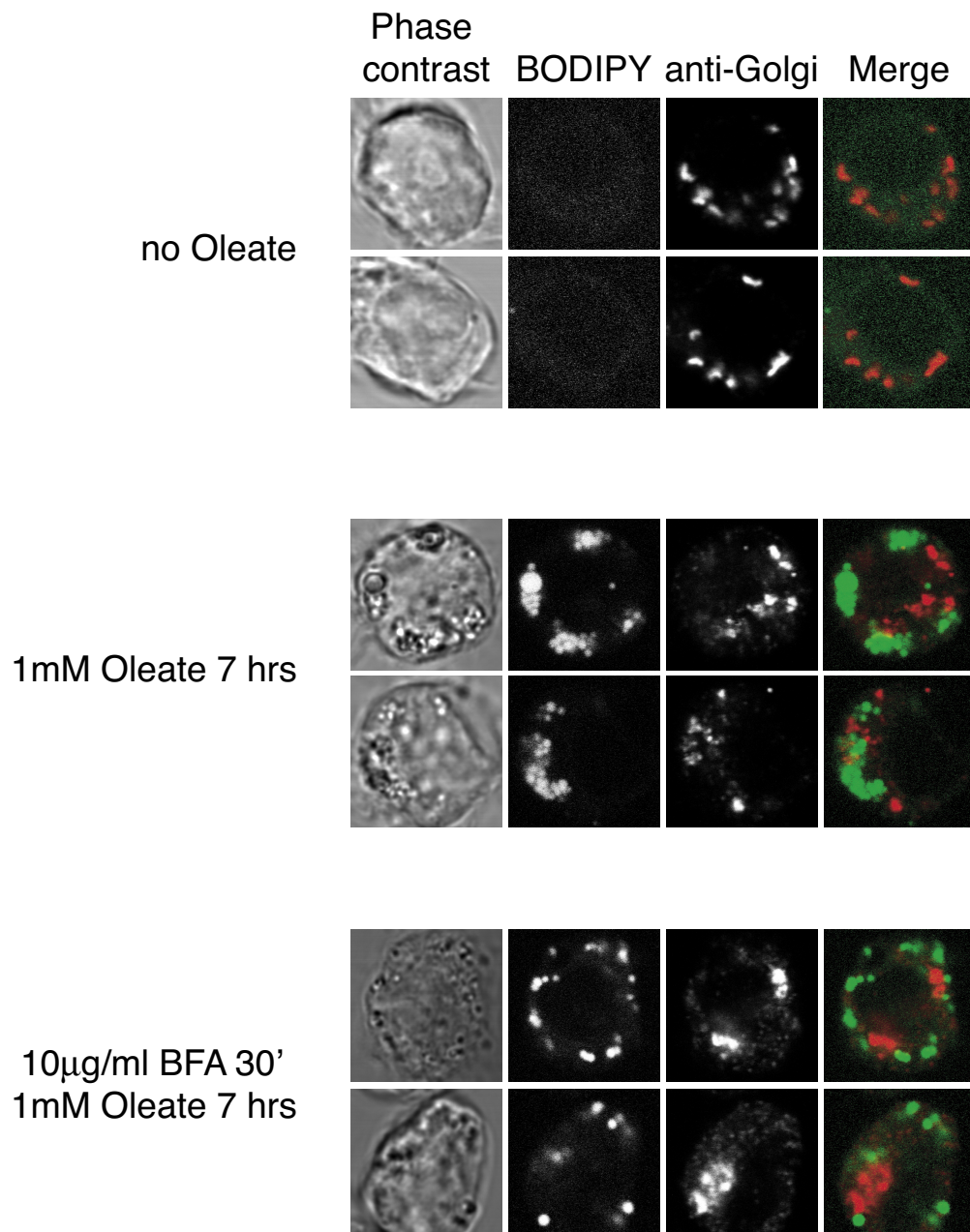


Farese *et al*, Figure S2



Farese et al, Figure S3

Farese *et al.*, Figure S4

Farese *et al*, Figure S5